[Danilo P. Mandic, Naveed ur Rehman, Zhaohua Wu, and Norden E. Huang]

Empirical Mode Decomposition-Based Time-Frequency Analysis of Multivariate Signals

Theory and Applications of Time-Frequency Analysis
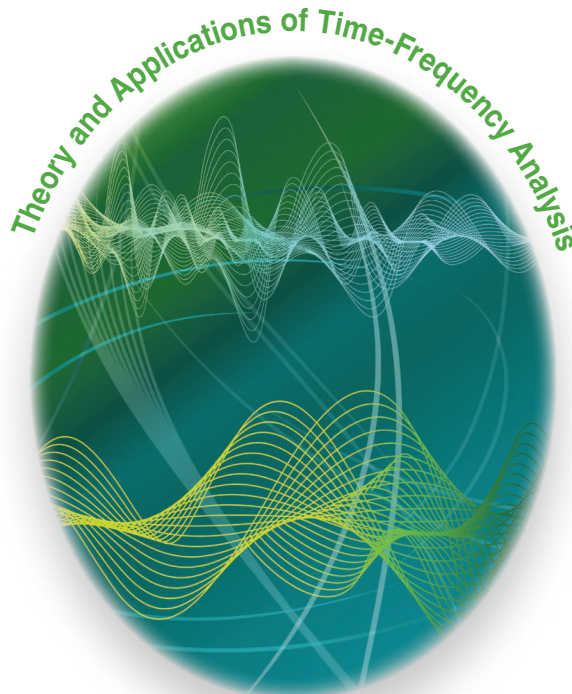
[The power of adaptive data analysis]

This article addresses data-driven time-frequency (T-F) analysis of multivariate signals, which is achieved through the empirical mode decomposition (EMD) algorithm and its noise assisted and multivariate extensions, the ensemble EMD (EEMD) and multivariate EMD (MEMD). Unlike standard approaches that project data onto predefined basis functions (harmonic, wavelet) thus coloring the representation and blurring the interpretation, the bases for EMD are derived from the data and can be nonlinear and nonstationary. For multivariate data, we show how the MEMD aligns intrinsic joint rotational modes across the intermittent, drifting, and noisy data channels, facilitating advanced synchrony and data fusion analyses. Simulations using real-world case studies illuminate several practical aspects, such as the role of noise in T-F localization, dealing

with unbalanced multichannel data, and nonuniform sampling for computational efficiency.

MOTIVATION FOR DATA-ADAPTIVE ANALYSIS

Advances in sensor technology have enabled routine recordings of both multidimensional (e.g., three-dimensional RGB images) and multichannel (e.g., sensor arrays) signals. Such data are typically nonlinear and nonstationary, and their rigorous T-F analysis requires a multiscale approach at the accuracy level of instantaneous frequency (IF), attained through knowledge of joint intrinsic oscillatory modes across the data channels. The IF is also essential for a meaningful interpretation of nonlinear processes (containing subharmonics). To that end, it is convenient to employ the Hilbert transform (HT) in conjunction with the data model [1]

$$x(t) = \sum_{m=1}^{M} c_m(t) = \sum_m a_m(t)\,\psi_m(t) \quad (+\, r \sim \text{residual}), \quad (1)$$

where $a_m \sim$ amplitude, $\psi_m \sim$ oscillations. Many representations based on (1) can be derived—for the Fourier transform, $\psi_m(t) = \exp(-j\omega_m t)$ and $a_m = \text{constant}$. However, the HT produces meaningful IF only for monocomponent data while

the Bedrosian and Nuttall theorems [2], [3] impose further constrains on the pair $[a_m, \psi_m]$, e.g., their nonoverlapping spectra. Quadratic Wigner–Ville methods provide excellent localization but allow for the analysis of only one frequency at a time, while hybrid methods [4] and filterbanks help to deal with nonstationary data statistics, but they too yield mathematical artefacts [5], [6].

The need to estimate IF of multivariate data can be justified on both mathematical and physical grounds (e.g., nonlinearity, variations in light and sound), yet standard tools either operate channel-wise thus not accounting for cross-channel information, or use static templates (basis functions) imposing nonexisting structure on data [7].

LIMITATIONS OF STANDARD METHODS

Exploratory T-F analysis of multivariate data is typically formulated through integral transforms and analytic signal representations [1], [8]. While convenient, this also poses severe limitations arising from the following:

■ *Fixed bases*: Standard Fourier and wavelet approaches employ predefined basis functions (harmonic, mother wavelet), e.g., a sum of sinusoids with fixed frequency, phase, and amplitude (Fourier). The accuracy thus critically depends on
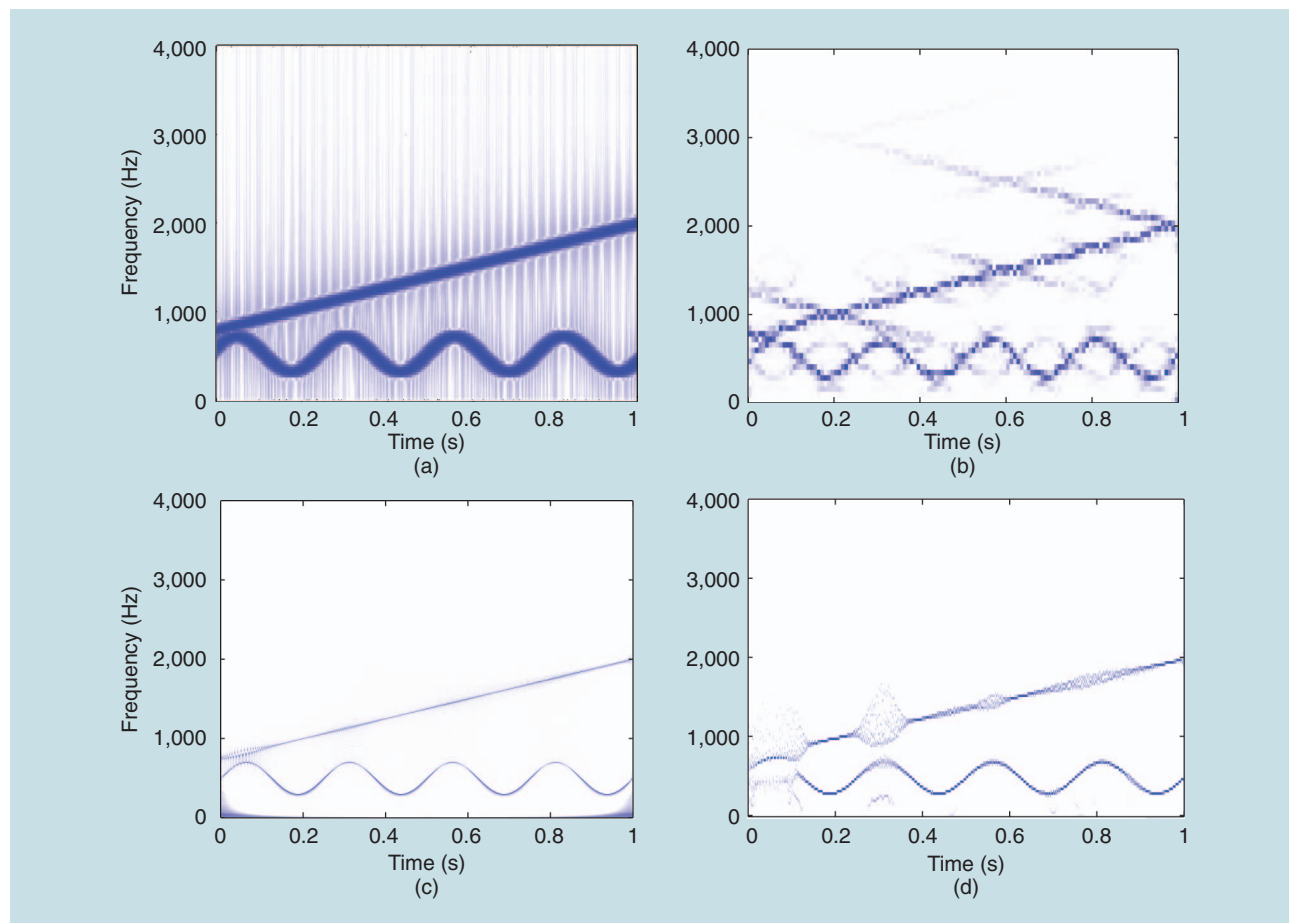
[FIG1] The T-F analysis of nonstationary signals: (a) STFT spectrogram, (b) wavelet packet, (c) synchrosqueezed transform, and (d) HHS.

data length and stationarity, yet patterns in real-world data can be short and intermittent.

■ *Uncertainty principle*: Integral transforms (Fourier, wavelet, Hilbert) blur the notion of time, thus compromising the analytic signal representation and trading the temporal resolution for frequency resolution.

■ *Physical insight*: A direct application of the analytic signal representation to nonmonocomponent data may produce negative IFs, with no justification in physics.

■ *Inadequate metrics*: Correlation, coherence, and synchrony measures are defined globally, however, patterns in data occur at their own intrinsic scales and thus accurate descriptors should be local and scale dependent.

ADVANTAGES OF DATA-DRIVEN APPROACHES

The EMD methods are nonparametric in the sense that the components $c_m(t)$ in (1) are derived empirically from the data and have the following desirable properties:

■ *Adaptivity*: The EMD bases are amplitude/frequency modulated (AM–FM) locally [10], [5], data-adaptive, and sparse [12], [13]. This facilitates the discovery of intrinsic patterns at multiple scales, while not requiring the rigid assumptions of harmonic or stationary data structures.

■ *Enhanced accuracy*: Through a template-free identification of the multiple within- and cross-channel scales in data, EMD promises the T-F accuracy at the IF level, and a natural account of inter- and intrawave modulations (nonlinearity).

■ *Integrity*: Coherent "instantaneous" treatment of multichannel information ensures the integrity of multivariate bases, thus facilitating synchrony, causality, and data fusion studies, while allowing for intrinsic, scale-dependent, data association metrics [9].

EMPIRICAL MODE DECOMPOSITION

The EMD models a signal x of length L as a sum of M oscillatory components called intrinsic mode functions (IMFs). These correspond to the bases $\{c_m\}_{m=1}^M$ in (1), and are sparse (with $M \ll L$), template free, and entirely data driven. Since the aim of EMD is for IMFs to represent intrinsic temporal modes (scales) that characterize the data, the residual r in (1) cannot contain a full oscillation and its role is to model the trend within a signal [10].

Recall that the estimation of IF via the HT gives 1) negative IF for data with a mismatch in the number of extrema and zero crossings, and 2) negative IF in the presence of a trend and dc offset. To resolve these issues, IMFs are required to be monocomponent and to have the following:

P1) symmetric upper/lower envelopes (zero mean) [11]

P2) the numbers of zero-crossings and extrema that are either equal or differ by exactly one.

Satisfying these conditions ensures narrowband (single-scale) IMFs that both admit the representation in (1) and also lend themselves to conveying physically meaningful information. Algorithm 1 summarizes the steps in EMD computation for a signal $x(t)$ initialized with $x'(t) = x(t)$ [10].

Algorithm 1: Sifting algorithm for EMD, for m = 1, ..., M

1) Find the locations of all the extrema of the variable $x'(t)$.

2) Interpolate (using local spline interpolation) between all the minima (cf. maxima) to obtain the lower (cf. upper) envelope connecting the minima, $e_{\min}(t)$ (cf. $e_{\max}(t)$).

3) Compute the local mean $m(t) = (e_{\min}(t) + e_{\max}(t))/2$.

4) Subtract the local mean from the loop variable $x'(t)$ to obtain the "modulated oscillation" $d(t) = x'(t) - m(t)$.

5) If $d(t)$ satisfies a stopping criterion (see below) set $\mathrm{IMF}_m = d(t)$, else set $x'(t) = d(t)$ and go to Step 1.

6) Subtract the so derived IMF from the variable $x'(t)$, so that $x'(t) := x'(t) - \mathrm{IMF}_m$ and go to Step 1.

7) Stop the sifting process when the residual from Step 6 becomes a monotonic function—the trend r in (1).

STOPPING CRITERIA

The stopping criterion in Step 5 of EMD checks if the "local trend" $d(t)$ fulfills the IMF properties P1) and P2). Its choice governs the accuracy of EMD—oversifted IMFs contain unwanted amplitude modulations, whereas undersifted IMFs tend to violate the monocomponent criterion. Existing stopping criteria are mostly empirical, and they may stop the sifting after, for instance:

■ the condition P2) for IMFs is met for K consecutive times; usually $4 \leq K \leq 8$ [14]

■ the lower and upper envelopes are symmetric [50].

Notice that condition P2) is almost equivalent to all local maxima being positive and all local minima negative.

ALTERNATIVE LOCAL MEAN ESTIMATION METHODS

More accurate local mean estimation—a key step within EMD—can be obtained by replacing splines in Step 2 of Algorithm 1 with, e.g., Hermite polynomials [36] or by using optimization [17], [18].

TIME-FREQUENCY VIA EMD: HILBERT–HUANG SPECTRUM

An attractive property of EMD is that its bases both model oscillations within their intrinsic "scale bandwidth" and also account for time-varying drifts, including those within a single cycle: so-called *intrawave modulations* (signatures of nonlinearity). In addition, the IMFs admit an amplitude-phase modulated representation $\mathrm{IMF}_m \approx a_m(t)\cos(\theta_m(t))$, where the amplitudes, $a_m(t)$, and phases, $\theta_m(t)$, are time varying. The IF can then be obtained through

■ a direct differentiation of the argument, $d\theta_m(t)/dt$

■ a combination with the quadrature $a_m(t)\sin(\theta_m(t))$, thus requiring a monocomponent signal [19]

■ analytic representation of IMFs as in (2).

The EMD embarks on the monocomponent nature of IMFs [conditions P1) and P2)] to estimate IF on an IMF-by-IMF basis from their analytic versions $\mathrm{IMF}_m + {}_j\mathcal{H}\{\mathrm{IMF}_m\} = a_m\exp({}_j\theta_m)$, where $\mathcal{H}\{\cdot\}$ is the HT operator. Such an analytic representation has the form in (1), i.e.,

$$z(t) = \sum_{m=1}^M a_m(t)\exp(j\theta_m(t)) = \sum_{m=1}^M a_m(t)\exp\left(j\int \omega_m(s)\,ds\right) \tag{2}$$

so that for each IMF the IF $\omega_m(t) = d\theta_m(t)/dt$. For real-world signals, the amplitudes are typically much less varying than the phases, thus giving physically meaningful values $\omega_m \geq 0$. The amplitudes $\{a_m(t)\}_{m=1}^M$ and instantaneous frequencies $\{\omega_m(t)\}_{m=1}^M$ plotted against time yield a T-F-amplitude representation of the signal, termed the *Hilbert–Huang spectrum* (HHS) [19].

Figure 1 shows T-F estimates for a nonstationary mixture of a linear chirp and FM sinusoid, obtained using the short-time Fourier transform (STFT), wavelet packet decomposition (WT), reassigned scalogram (spectrogram using wavelets) within the synchrosqueezed wavelet transform (SST), and the HHS. Notice the artefacts present in the fixed-bases STFT and WT, and enhanced T-F tracking when using EMD and the EMD-like SST [5].

Figure 1 illustrates the advantages of EMD, such as its locality, ability to operate on nonstationary data, and approach the accuracy level of IF, but the graphs also point out that EMD is most successful when the signal has well-separated frequency components. This is exemplified by the T-F artefacts in the region where the chirp frequency was less than twice the frequency of the FM signal (up until 0.35 s) [20], despite the actual reconstruction based on (2) still being perfect. The fixed-basis STFT and WT could not cope with nonstationarity and produced harmonics and spurious frequencies, while the SST— a "posterior" method that reallocates WT coefficients to have concentrated T-F representation—was not immune to these effects either [21].

Figure 2 further illuminates the issue of "one-or-two-components" for the two-tone signal $s(t) = \cos(2\pi t) + 0.5\cos(2\pi\,0.7t)$ for which $f_{high}/f_{low} < 2$. The SST produced two distinct lines in the T-F plane, but also created rippling artefacts, while the EMD correctly interpreted the signal as a single component with an intrawave element—a perfectly valid AM-type IMF arising through heterodyning of the two closely spaced tones, whereby $\cos\alpha\cos\beta = (1/2)[\cos(\alpha - \beta) + \cos(\alpha + \beta)]$. Heterodyning routinely occurs in nonlinear and physiological systems, e.g., at the contact between metal electrodes and skin (via conductive gel); the original tones can be recovered either through a demodulation of IMFs or by using a masking signal [22].

NOISE-AIDED EMD COMPUTATION: THE EEMD

The success of EMD has also highlighted that for intermittent data, despite a perfect reconstruction, EMD may suffer from

- *mode mixing*, whereby either an IMF contains different oscillatory modes, or one mode is in different IMFs
- *aliasing*, i.e., the overlapping of IMF spectra caused by a sub-Nyquist nature of extrema sampling [16].

Mode mixing thus obscures the physical meaning of IMFs and also violates the local orthogonality of IMFs, while the cubic spline interpolation is not an ideal filter and contributes to aliasing. In addition, a sufficient number of extrema is needed for successful envelope fitting within EMD, thus the lack of extrema at the very beginning and end of a data segment creates the so-called *end effect artefacts*, which is visible in Figure 1.

To help overcome these issues, the EEMD algorithm by Wu and Huang [23], described in Algorithm 2, employs ensemble
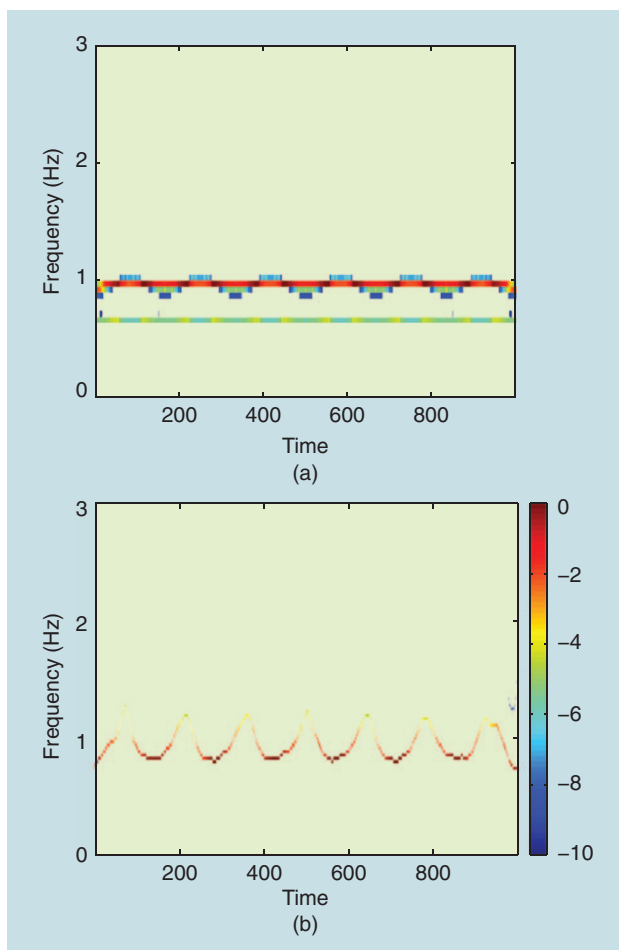

[FIG2] Separation of closely spaced tones by SST and EMD: (a) rippling artefacts when using SST and (b) one compact AM component produced by EMD.

averaging of noisy signal realizations, whereby EMD is applied to every member of the ensemble

$$\text{Ensemble:}\quad \{s_n(t)\}_{n=1}^N = x(t) + \{w_n(t)\}_{n=1}^N, \qquad (3)$$

where $x(t)$ is the original signal, $\{w_n(t)\}_{n=1}^N \sim \mathcal{N}(0, \sigma^2)$ are independent realizations of white Gaussian noise (WGN), and the averaging is performed across same-index IMFs over the
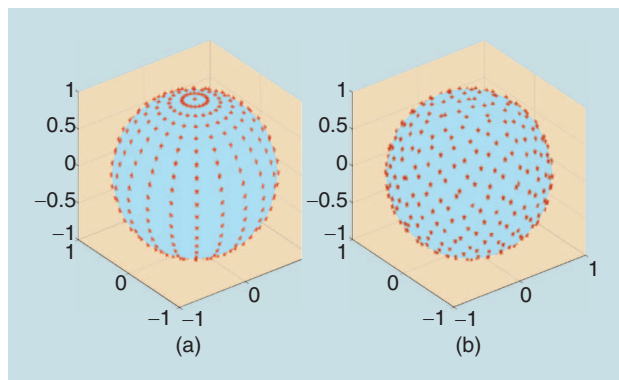
[FIG3] Direction vectors for the projections of trivariate data: (a) angular sampling and (b) uniform sampling.

ensemble. The EEMD helps mitigate mode mixing by virtue of the dyadic filterbank property of EEMD for WGN (explained later), while aliasing is dealt with through much more detailed envelopes owing to extrema in added noise.

Algorithm 2: EEMD

1) Generate the ensemble $s_n(t) = x(t) + w_n(t)$ for $n = 1, \ldots, N$, where $w_n(t) \sim \mathcal{N}(0, \sigma^2)$.

2) Decompose every member of the ensemble $s_n(t)$ into M_n IMFs using standard EMD, to yield the set $\{c_m^n(t)\}_{m=1}^{M_n}$.

3) Average same-index IMFs $c_m^n(t)$ across the ensemble to obtain the IMFs within EEMD; for instance, the mth IMF is obtained as $\bar{c}_m(t) = (1/N) \sum_{n=1}^{N} c_m^n(t)$.

Since through averaging the effects of added WGN reduce with an increase in the ensemble size N according to σ^2/N, the EEMD benefits from enhanced local mean estimation in noisy data to yield IMFs that are less prone to mode mixing. This has made EEMD a major algorithm to robustly perform EMD, at a cost of increased computational complexity.

MULTIVARIATE EMD

Multivariate data contain joint rotational modes (generalized oscillations), whose coherent treatment is required for meaningful T-F estimation. Univariate EMD algorithms applied channel-wise may yield useful results for loosely coupled data channels, however, in general this approach is hindered by

- *Nonuniformity*: Standard EMD is not likely to yield the same number of IMFs for every data channel.
- *Scale alignment*: There is no guarantee that same-index IMFs would contain equal scales across data channels.
- *Nature of IMFs*: Enforcing the same number of IMFs for every data channel may compromise T-F estimation, as such IMFs are typically not monocomponent.

Not surprisingly, the issues of common mode alignment and nonuniqueness have been major obstacles for a more widespread use of EMD in studies that require same-index IMFs containing the information pertaining to the same scale (synchrony, causality, data/image fusion) [24].

Direct MEMD algorithms were first developed for the bivariate (complex) case and include the complex EMD [25], which exploits univariate analyticity of data channels but does not guarantee coherent bivariate IMFs, and the bivariate EMD (BEMD) [26], which applies standard EMD to multiple data projections and averages the so-obtained local means to yield the true bivariate local mean. The BEMD employs uniform data projections on a unit circle, and its accuracy increases with the number of projections, while the rotation-invariant EMD (RI-EMD) uses the same principle as BEMD, albeit with only two projections in opposite directions [27].

MEMD PRINCIPLE

For multivariate data, the principle of separating oscillations that underpins EMD should be generalized to that of separating rotations, whereby
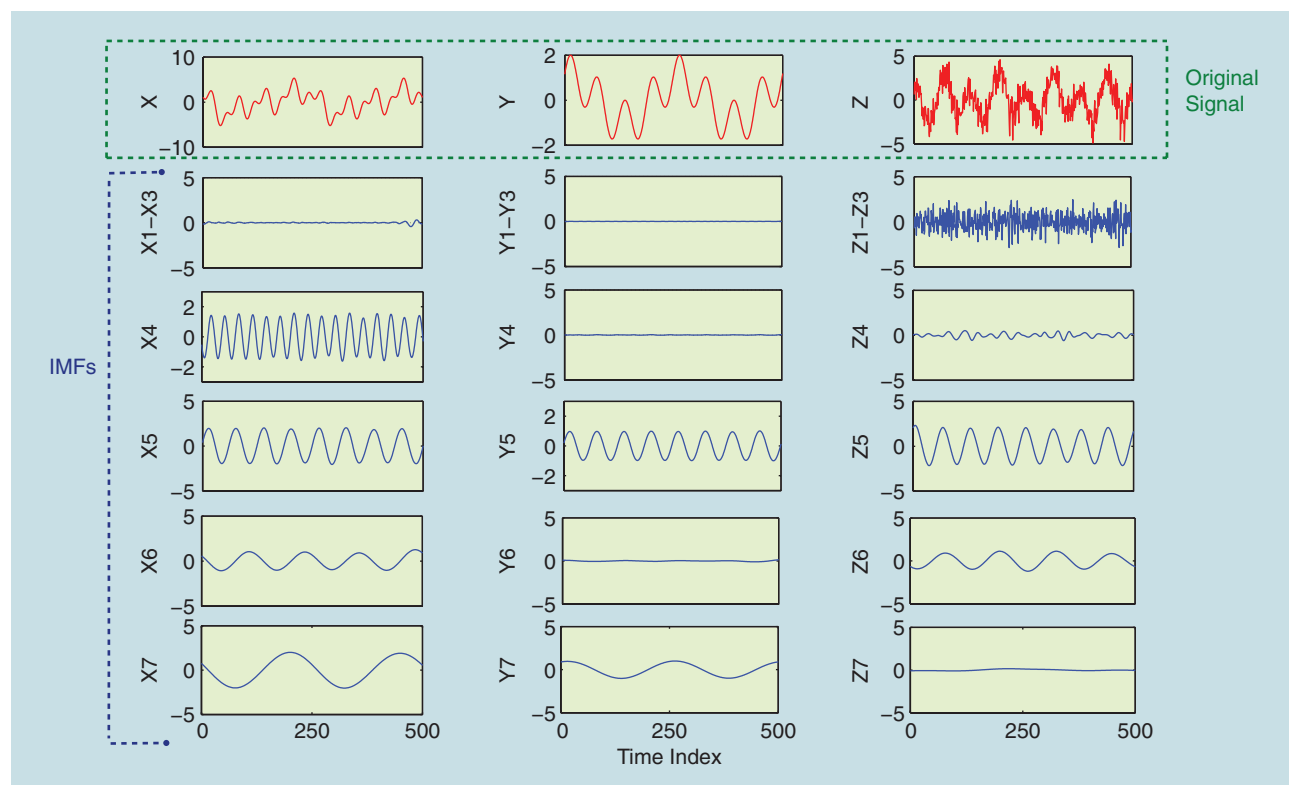
[FIG4] MEMD applied to a trivariate tone-noise mixture, giving perfectly aligned intrinsic modes in the *X, Y, Z* channels.
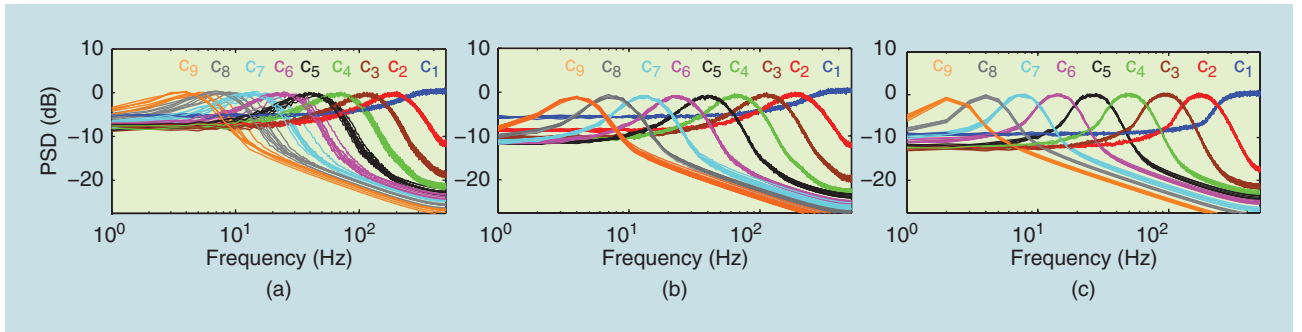
[FIG5] The EMD as a filterbank. The spectra of IMFs for (a) standard EMD, (b) EEMD, and (c) MEMD.

EMD: signal = slow oscillation + fast oscillation
MEMD: signal = slow rotation + fast rotation. (4)

To this end, the MEMD [28] uses a vector-valued form of (1) to decompose a p-variate signal $\mathbf{s}(t)$ as

$$\mathbf{s}(t) = \sum_{m=1}^{M} \mathbf{c}_m(t) + \mathbf{r}(t), \qquad \mathbf{s}, \mathbf{c}_m, \mathbf{r} \in \mathbb{R}^p, \qquad (5)$$

where the p-variate IMFs, $\{\mathbf{c}_m\}_{m=1}^M$, contain scale-aligned intrinsic joint rotational modes and $\mathbf{r}$ is the residual.

MULTIDIMENSIONAL LOCAL MEAN
The MEMD estimates the local p-dimensional mean through averaging of multiple envelopes obtained by taking signal projections along multiple uniformly distributed directions in the p-dimensional space, and subsequently interpolating (via cubic splines) their extrema. Generalizing the principle behind BEMD, the direction vectors are governed by an appropriate sampling of a p-dimensional hypersphere. Therefore, the accuracy of local mean calculation depends both on the distribution and number of direction vectors, becoming critical for a small number of projections (see the section "Practical Issues in Using EMD").

Figure 3(a) depicts a nonuniform sampling scheme based on spherical angles [29], while Figure 3(b) illustrates uniform sampling [28] for projection vector directions generated by low-discrepancy Hammersley sequences [30] (quasi-Monte-Carlo sampling). Algorithm 3 summarizes the operation of MEMD for a p-variate signal $\mathbf{s}(t)$, whereby a uniform sampling scheme is preferred to assign equal weighting to all the projection directions, unlike the angular sampling which favors the poles of the sphere in Figure 3(a).

The ability of MEMD to identify and align intrinsic rotational modes is illuminated in Figure 4 for a trivariate signal $s = [X, Y, Z]$ whose components are mixtures of an 8-Hz sinusoid common to all data channels, a 16-Hz tone in the X-component, and 4-Hz and 2-Hz tones in the X&Z and X&Y components; the Z-component was also contaminated by noise. Notice that all IMFs are three-dimensional and scale aligned: the 8-Hz tone present in all data channels is localized in a single IMF5 = [X5, Y5, Z5], while the 16-Hz, 4-Hz, and 2-Hz tones are localized in IMF4, IMF6, and IMF7, respectively, whereas the noise is located in IMF1–IMF3.

Algorithm 3: MEMD

1) Generate a V-point Hammersley sequence used for uniformly sampling a p-dimensional sphere [Figure 3(b)].
2) Calculate the projections $q_{\theta_v}(t)$ of the signal $\mathbf{s}(t)$ along the direction vector $\mathbf{x}_{\theta_v}$, for $v = 1, \ldots, V$ to give the set of projections $\{q_{\theta_v}(t)\}_{v=1}^V$.
3) Find the time instants $\{t_{\theta_v}^i\}_{v=1}^V$ corresponding to the maxima of the set of projected signals $\{q_{\theta_v}(t)\}_{v=1}^V$.
4) Interpolate $[t_{\theta_v}^i, \mathbf{s}(t_{\theta_v}^i)]$ to obtain the multivariate envelope curves $\{\mathbf{e}_{\theta_v}(t)\}_{v=1}^V$.
5) Calculate the mean of the V multidimensional envelopes

$$\mathbf{m}(t) = \frac{1}{V} \sum_{v=1}^{V} \mathbf{e}_{\theta_v}(t). \qquad (6)$$

6) Extract the "detail" $\mathbf{d}(t) = \mathbf{s}(t) - \mathbf{m}(t)$. If $\mathbf{d}(t)$ fulfills the stoppage criterion for a multivariate IMF, apply the above procedure to $\mathbf{s}(t) - \mathbf{d}(t)$, else repeat for $\mathbf{d}(t)$.

Such a strict mode alignment is not achievable when applying standard EMD channel-wise, highlighting the following desirable properties of MEMD:

■ Data are analyzed in the very p-dimensional domain where they reside, preserving joint channel properties.
■ The p data channels have the same number of scale-aligned IMFs, containing same rotational modes (integrity of scales).
■ Should mode mixing occur, same-index IMFs will still contain aligned composite scale(s), making possible coherent multivariate T-F analysis.

These properties facilitate the use of MEMD in various multichannel synchrony, coherence, and data fusion applications [24].

NOISE-ASSISTED MEMD
The success of EMD and EEMD has also highlighted that

■ adding noise to data may both increase the residual error and produce different number of IMFs for ensemble members in (5), compromising the IMF alignment across data channels
■ the nonlinearity of EMD implies that an ensemble averaged IMF within EEMD is not necessarily an IMF.

The idea behind noise-assisted MEMD (NA-MEMD) is not to directly add noise to n-channel multivariate data, but to create an $(n + l)$-dimensional "composite" space comprising the

n-dimensional signal subspace and an adjacent subspace of l-independent WGN realizations [31]. The subsequent application of MEMD yields $(n + l)$-variate coherent IMFs whose integrity is reinforced by the filterbank property of MEMD for WGN (see Figure 5). The n-variate IMFs corresponding to the original signal are then extracted from the $(n + l)$-variate IMFs by discarding the l channels pertaining to the noise subspace. The disjoint nature of the signal and noise subspaces also helps reduce residual noise and mode mixing in the NA-MEMD.

FILTERBANK PROPERTY OF EMD
An important property of EMD algorithms is that the IMFs exhibit a quasi-dyadic filterbank structure for WGN (similar to wavelets), as shown in Figure 5 for EMD, EEMD, and MEMD. The plots were averaged over N = 100 realizations of an eight-channel WGN process of length L = 1,000 to which MEMD was applied directly and the univariate EMD and EMMD channelwise. The scale-aligned IMFs within MEMD gave better defined subband filters as compared with EMD and EEMD. This property also explains enhanced T-F localization of noise-aided EMD algorithms [15], [31].

MODE ALIGNMENT
Accurate IF estimation based on (2) requires the data-driven basis functions within EMD to be approximately monocomponent and locally orthogonal. The EMD algorithms do yield such bases: Figure 6 shows correlations of normalized IMFs (performed channel-wise) averaged over N = 1,000 realizations of bivariate WGN of length L = 1,000, with bivariate MEMD [Figure 6(a)] outperforming standard EMD applied channel-wise [Figure 6(b)].

Although both EMD and BEMD produced diagonally dominant correlograms of IMFs, since within BEMD same-index bivariate IMFs contain the same scale, the correlogram of bivariate IMFs [Figure 6(a)] exhibits a more pronounced diagonal dominance (reduced leakage), highlighting that

- cross-correlation between IMFs (cf. leakage between subbands in Figure 5) may cause blurred T-F estimates
- the almost orthogonal IMFs (sharp filterbank) within MEMD yield aligned scales but also tend to filter out harmonics for close scales, while the EMD filterbank exhibits leakage but accommodates nonlinear signals.

MULTIDIMENSIONAL EMD FOR IMAGES
The success of EMD in identifying multiple intrinsic scales in univariate data has motivated its extensions to images, surfaces, and volumes. Fitting of such multidimensional envelopes is not straightforward (presence of saddle points, ridges, valleys, sharp edges), and EMD-based image analysis methods employ
- Class I1: long vectorization by concatenating, e.g., all the rows
- Class I2: short vectorization, by treating every row (cf. column) of an image as a separate univariate signal
- Class I3: direct multidimensional surface fitting.

Long vectorization blurs spatial dependencies in an image while short vectorization produces image "slices" to give "pseudo-bidimensional" IMFs. An "image-EMD" should therefore 1) identify the extrema of an image, 2) interpolate the upper and lower image envelopes, 3) average the envelopes to give a local mean, and 4) continue as in EMD [32]. The bidimensional EMD belongs to Class I3 [33] and interpolates image extrema though radial basis functions (tensor product) or B-splines (Class I2), using the Riesz transforms instead of the HT to compute the local wave number. The method by Linderhed [32] uses thin-plate splines for the interpolation of the extrema; this is a "meshless" method giving two-dimensional (2-D) IMFs and a more accurate compression than wavelets, while EMD for surfaces [34] also uses geodesic operators. Both require constrained optimization to preserve sharp edges, and are sensitive to noise and extrema definition [35]. A computationally effective method in [36] produces 2-D IMFs by combining Delaunay triangularization with cubic interpolation,
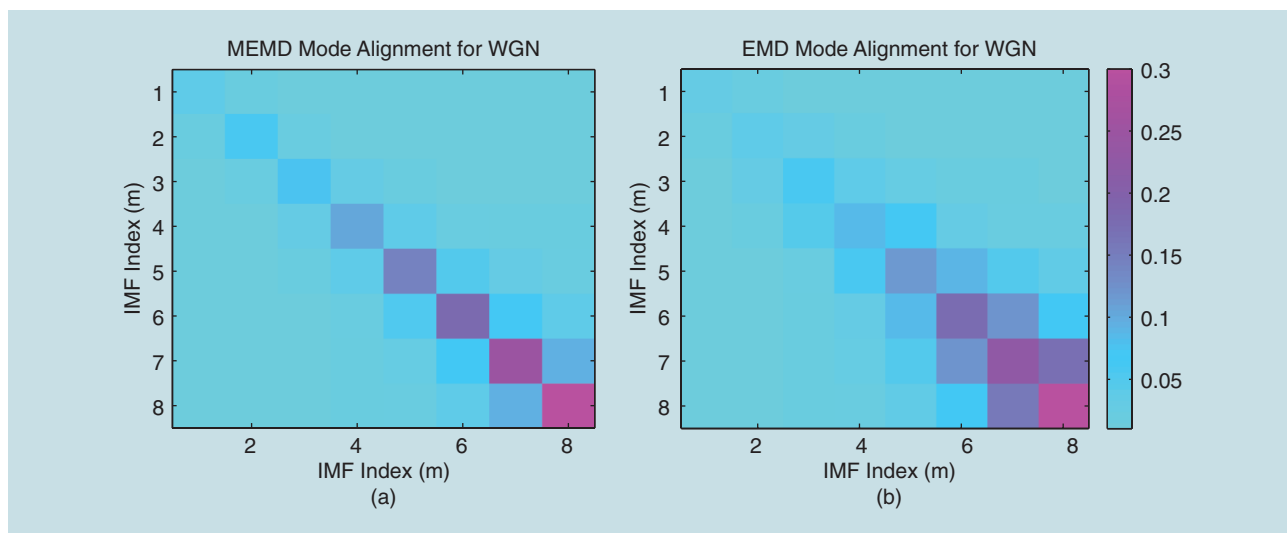
[FIG6] Cross-correlations of normalized IMFs for bivariate WGN. (a) BEMD. (b) Channel-wise EMD.
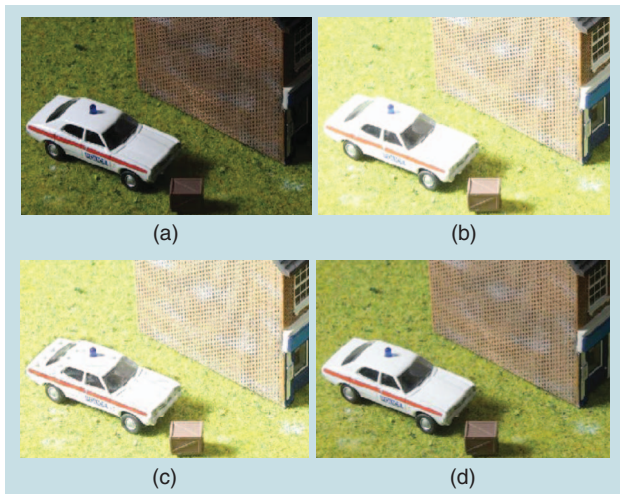
[FIG7] An image fusion example. Parts (a) and (b) are original out-of-exposure images. Part (c) is the wavelet-based fusion (five level sets). Part (d) is the MEMD-based fusion (64 projection directions).

while a related method in [37] employs a mesh fitting method based on finite elements to compute the local mean, rather than using envelope interpolation.

The multidimensional EEMD (MEEMD) [39] applies EEMD to both horizontal and vertical image slices to reduce mode mixing and produce well-defined scales. For an (M × N)-pixel image, the EEMD is first applied, e.g., to the M rows slice-by-slice. The subsequent M univariate EEMDs are ensemble-averaged in an IMF-by-IMF fashion to yield J horizontal scales of the original image. The N columns of these (M × N)-dimensional "pseudoimages" are then treated as slices and decomposed in the same way via separate EEMDs to give K IMFs that capture the vertical spatial scales, a total of (J × K) pseudoimages. Coherent 2-D IMFs are obtained by recombining the x- and y-scales; the MEEMD also scales to volumes of any dimension.

Figure 7 illustrates the performance of the MEMD and discrete wavelet transform (DWT) for the fusion of overexposed and underexposed color images (Class I1). Incorrect exposure blurs the detail and both the DWT- and MEMD-based fusion schemes were able to enhance the images. The DWT produced visible artefacts along the car edges and for flat panels (patches on the car boot and roof), while the MEMD-fused image was artefact free [24] (for stopping criteria, see [51]).

THE ROLES OF INTERMITTENCY AND NOISE

The intermittency of real-world data is a main cause of mode splitting and mode mixing in EMD; mode splitting is manifested by the spread of one scale over two or more IMFs, while mode mixing refers to one IMF containing different scales [see Figure 8(a)]. In addition, the original EMD is compromised for relatively flat signals, with scarce extrema [50], [36], since this grossly affects the envelope interpolation—a key step in EMD. Noise-assisted EMD algorithms have the ability to mitigate this problem through the many additional local extrema arising due to the use of noise in the decomposition.
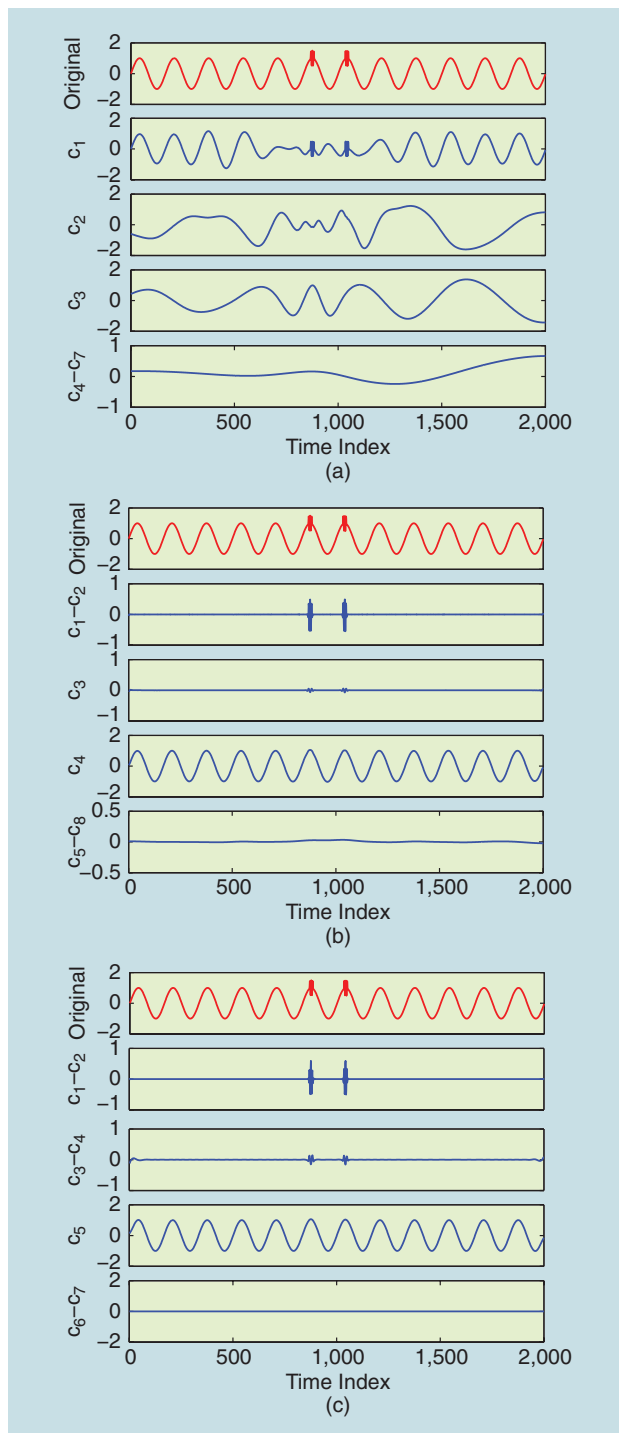
[FIG8] EMD decompositions of a sinusoid contaminated with intermittent interference, located on both sides of the sample 1,000. Standard EMD exhibited mode splitting in all IMFs, while EEMD and NA-MEMD correctly localized the sinusoid within a single IMF. (a) Standard EMD. (b) EEMD. (c) NA-MEMD.

CALCULATING EMD VIA NA-MEMD

Figure 8 illustrates the benefits of calculating univariate EMD via noise-assisted EMD algorithms on an example of a 2-Hz sinusoid corrupted by an intermittent interference. The original sinusoid satisfies the IMF conditions P1) and P2) and should be localized in

only one IMF, however, for the case of EMD, mode mixing occurred in IMF3 and IMF4 and mode splitting in IMF1–IMF3. The noise-assisted EEMD and NA-MEMD were able to localize the monocomponent sinusoid within a single IMF, with NA-MEMD exhibiting less residual noise than EEMD, whose IMFs c_5-c_8 still contained oscillations. The ensemble size for EEMD was N = 1,000 with the 6.98 dB signal-to-noise power ratio ($\sigma_w^2 = 0.2\sigma_x^2$), while for NA-MEMD, $l = 2$ adjacent noise channels were used to create a trivariate signal, with the signal-to-noise channel power ratio of 26 dB ($\sigma_w^2 = 0.02\sigma_x^2$).

REAL WORLD EXAMPLES

The advantages of noise-assisted and MEMD approaches over channel-wise univariate ones in T-F analysis of multivariate data are next illustrated in two examples of electroencephalogram (EEG) analysis for brain–computer interface (BCI). We considered seven EEG channels from the following experiments:

■ Experiment 1: a 15-Hz steady-state visual evoked potential (SSVEP), induced in EEG by a 15-Hz flashing visual stimulus

■ Experiment 2: motor imagery BCI, where a drifting $\mu \approx$ 10-Hz rhythm occurs when a subject imagines limb movement.

Figure 9 illustrates the EMD-based localization of the 15-Hz SSVEP by 1) averaging standard EMDs applied to the seven-variate EEG channel-wise and 2) nine-variate NA-MEMD (seven EEG channels and two noise channels). Both localized the 15-Hz SSVEP response, however, while as desired, each IMF within NA-MEMD contained a single scale the IMF spectra of univariate EMDs overlapped [e.g., IMF4 and IMF5 in Figure 9(a); see also Figure 6].

Within a similar setting, Experiment 2) aims to perform T-F localization of a real-world drifting 10-Hz μ-rhythm in EEG. Observe the blurred estimates when this nonstationary rhythm was analyzed using STFT and WT [Figure 10(a) and (b)], while the SST and NA-MEMD [Figure 10(c) and (d)] were able to track the IF in noisy EEG highly accurately and with continuous resolution (see also Figure 8).

PRACTICAL ISSUES IN USING EMD

UNBALANCED MULTIVARIATE DATA

Real-world multivariate data typically have noncircular (rotation-dependent) distributions, manifested in different power levels (and/or correlation) across the constitutive data channels; this biases standard Hilbert-based T-F estimation [45] and can even yield physically meaningless negative IF [44].

MEMD approaches employ uniform sampling for finding directions of data projections, a perfect match for circular data with equal channel powers, as shown in blue in Figure 11(a). For unbalanced data (improper, correlated), the density of projections within MEMD should match the signal dynamics, as illustrated in green in Figure 11(a) for a noncircular bivariate signal. Figure 11(b) and (c) considers uniformly and adaptively sampled noise-assisted BEMD (NA-BEMD) for a bivariate x = [signal; noise] Doppler radar signature, at an SNR of 8 dB. The data-adaptive sampling accounted for data noncircularity and gave a more accurate object motion signature [40] than the wavelet- and Fourier-based methods in Figure 12.

### CALCULATION OF INSTANTANEOUS FREQUENCY

While the analytic signal in (2) generates a unique pair $[a_m(t), \theta_m(t)]$ from the data (removing the ambiguity of many such combinations representing the data), an IMF is not necessarily monocomponent, violating the Bedrosian conditions [2]. However, the recent normalized HT (NHT) and direct quadrature (DQ) methods, in conjunction with EMD, have overcome the Bedrosian and Nuttall restrictions [19]. Multivariate T-F analyses based on EMD also help with this problem, as cross-channel information reinforces monocomponent IMFs, thus admitting correct application of HT, accurate IF calculation, and physically meaningful IMFs, as shown in Figures 8 and 9.

DATA-LENGTH EFFECTS

The resolution of Fourier and wavelet methods critically depends on data length, while EMD suffers from the end-effects ambiguity but copes well with short data [43], as shown in the image fusion example in Figure 7. This is further illustrated in Figure 12 for the example from Figure 11—both the WT and SST produced blurred T-F estimates for short data
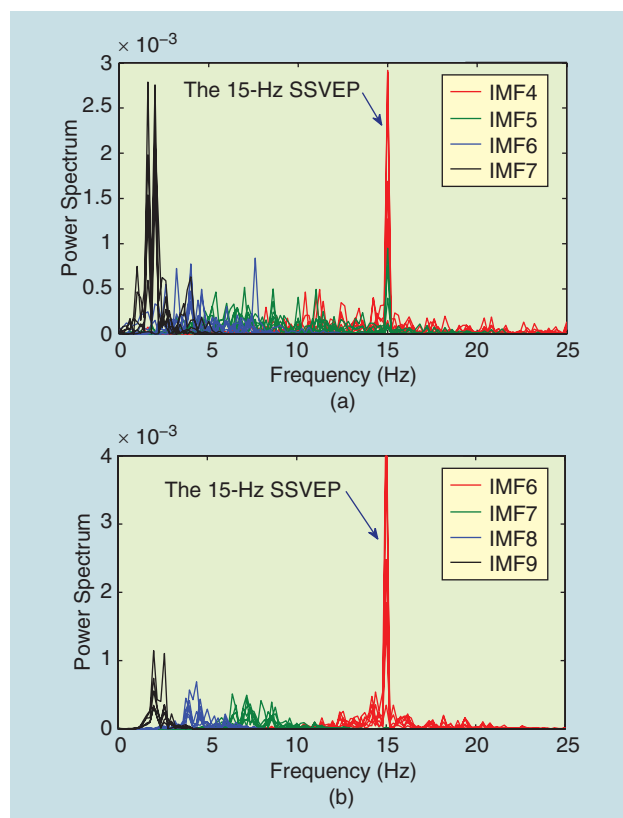
Power spectra of IMFs for a seven–channel SSVEP at 15 Hz from (a) channel-wise EMD and (b) multivariate NA-MEMD.
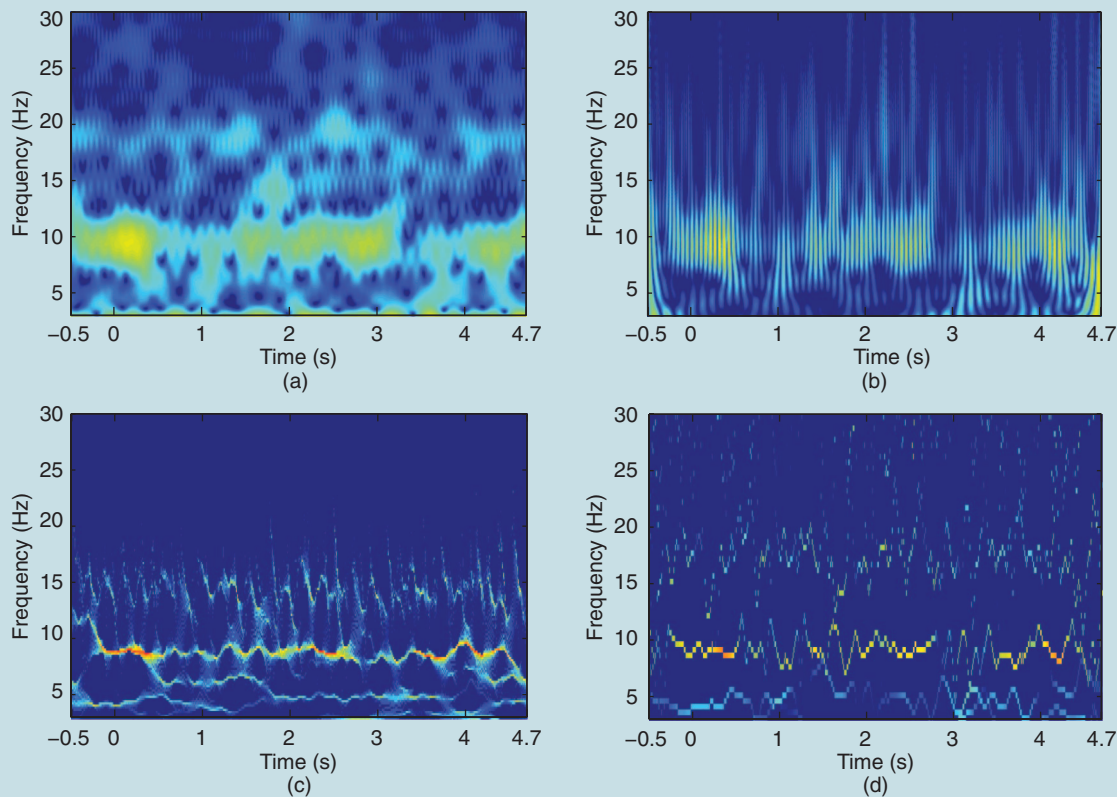
[FIG10] IF analysis of a drifting 10-Hz μ-rhythm in a motor imagery BCI. (a) Short-time Fourier transform. (b) Wavelet transform. (c) Synchrosqueezing transform. (d) NA-MEMD.

segments, while the NA-MEMD in Figure 11(c) had good resolution and gave plenty of detail.

PHYSICAL MEANING OF IMFs

We next illustrate that for real-world data whose intrinsic modes are nonstationary but with well-defined and nonoverlapping bandwidths, EMD approaches are capable of producing physically meaningful IMFs. Indeed, many natural signals, such as those coming from a living organism or environment, exhibit well-separated scales. For instance, human physiological responses occupy the following bands: <1 Hz for respiration, 1–2 Hz for pulse or eye blinks (EMG), while the EEG spectrum is divided into the nonoverlapping delta band centered around 4 Hz and the alpha band centered around 10 Hz and so on. Figure 13 compares the localization ability of independent component analysis (fastICA, routinely used in EEG analysis) and MEMD for the separation of <2 Hz eye movement artefacts (EMG) and the (8–13 Hz) alpha rhythm from background EEG. The subject moved their eyes throughout the recording, closing eyes after 10 s to induce the alpha activity in EEG [Figure 13(a)]. The extracted independent components (ICs) provided good reconstruction but no physical meaning, as their spectra [Figure 13(a)] did not represent either the EMG or alpha bands of interest [47]. On the contrary, the IMFs within MEMD were physically meaningful and perfectly captured

both the alpha rhythm and EMG frequencies in the corresponding nonoverlapping IMFs [Figure 13(b)].

ENVELOPE INTERPOLATION AND THE ROLE OF POSTPROCESSING

Envelope fitting underpins the EMD algorithm and is computationally demanding. For efficient computation, it is desirable to perform less accurate but affordable envelope interpolation followed by simple postprocessing [41]. Table 1 shows that when applied to adaptive forecasting, this approach outperformed standard cubic spline interpolation in terms of the prediction gain $R_p = 10 \log (\text{signal power/error power}) [\text{dB}]$. The imperfect IMFs obtained through piecewise linear extrema interpolation were enhanced by an M-channel adaptive filter of length P trained by the normalized least mean square (NLMS).

[TABLE 1] NLMS-EMD PERFORMANCE IN R_p FOR FILTER LENGTH P.

| TIME SERIES	INTERPOLATION	$P = 2$	$P = 5$	$P = 10$
HENON MAP	LINEAR	14.1	14.6	14.4
	CUBIC SPLINE	13.8	14.0	13.8
MACKEY GLASS	LINEAR	19.9	18.8	18.9
	CUBIC SPLINE	18.2	17.8	18.5
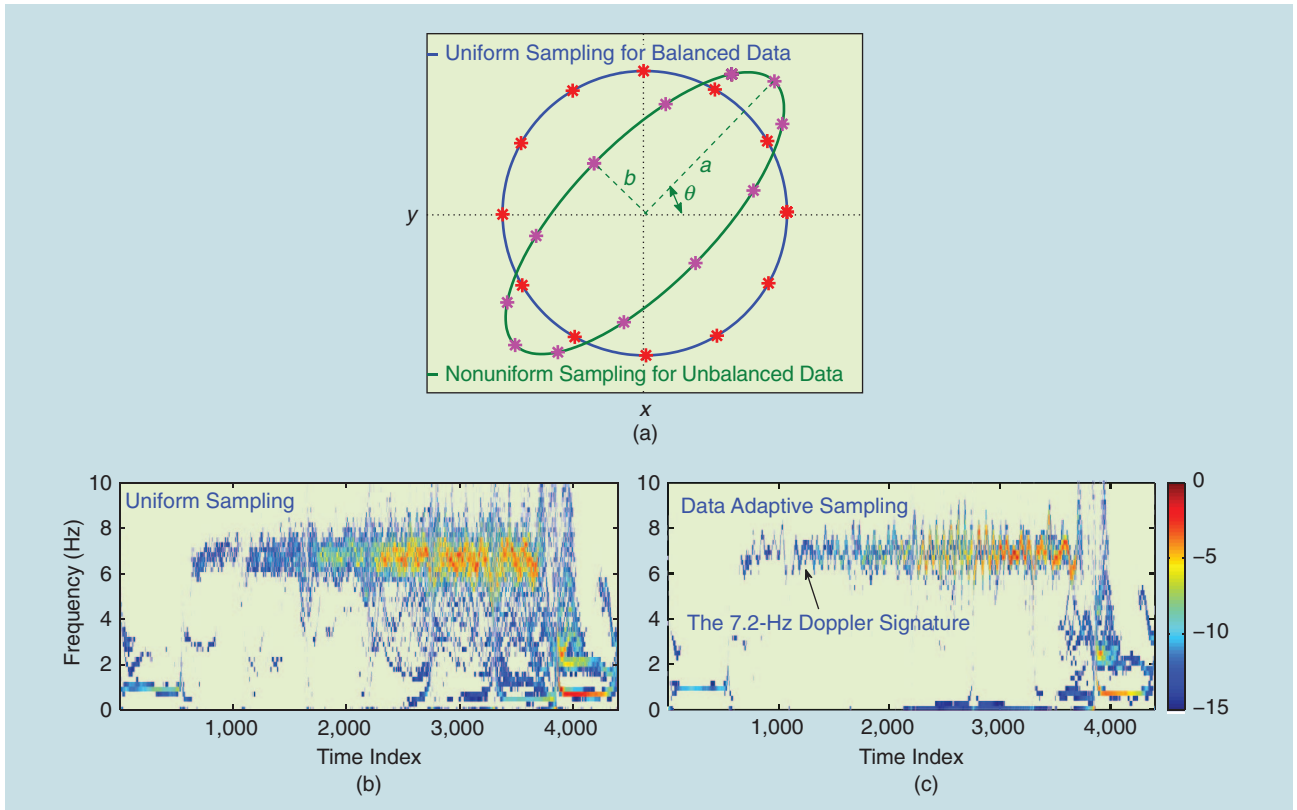
[FIG11] The T-F analysis of the Doppler signature of a moving object traveling at 10.2 cm/s toward the radar, causing a 7.2-Hz Doppler frequency shift. The NA-MEMD with data-adaptive sampling localized successfully the useful signal. (a) Unbalanced data projections. (b) NA-BEMD (uniform sampling). (c) NA-BEMD (data-adaptive sampling).

CONCLUSIONS AND FUTURE DIRECTIONS

EMD is a spontaneous multiresolution method that represents nonlinear and nonstationary data as a sum of oscillatory modes inherent in the data, called IMFs. In this way, EMD provides a sparse representation as IMFs are only required to be monocomponent, with no restrictions on linearity or stationarity. Like any other T-F technique, the success of EMD is context dependent: it is enormously useful for real-world data that have well-separated scales, such as physiological and environmental signals, yielding high-resolution IF estimates via the HHS.

For scenarios for which EMD is a good match, the IMFs are also likely to convey physical meaning, as in Figure 13, however, this cannot be generalized to wideband data or multiple closely spaced tones without an insight into the physics behind data generation. For instance, EMD will represent two closely spaced tones as an AM signal, as shown in Figure 2—this is physically perfectly meaningful, and we can isolate the two tones as long as we know
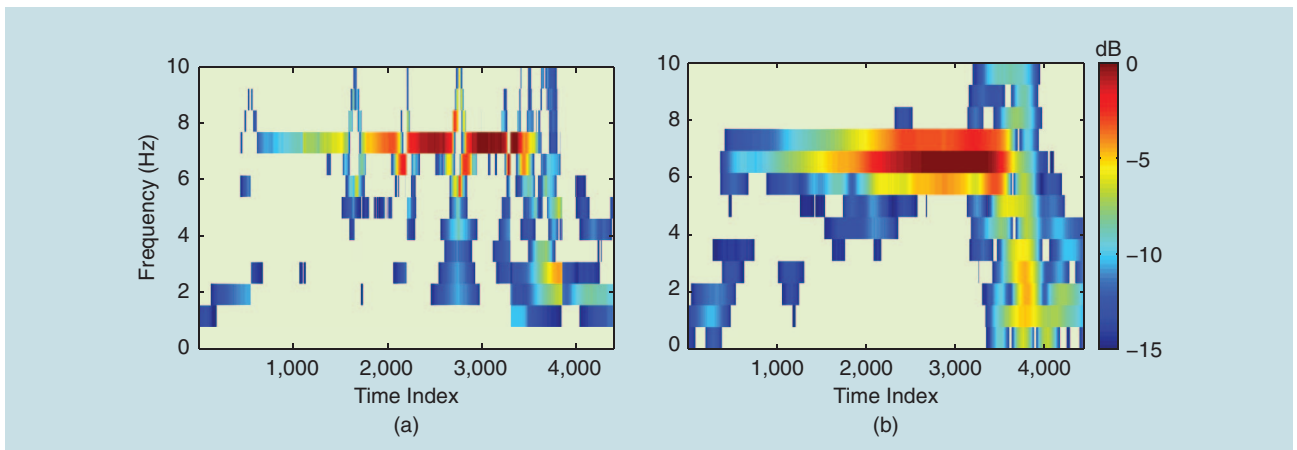
[FIG12] The performance of SST and WT for the example in Figure 12, using nonoverlapping segments of $L = 550$ samples: (a) synchrosqueezing transform and (b) short-time Fourier transform.
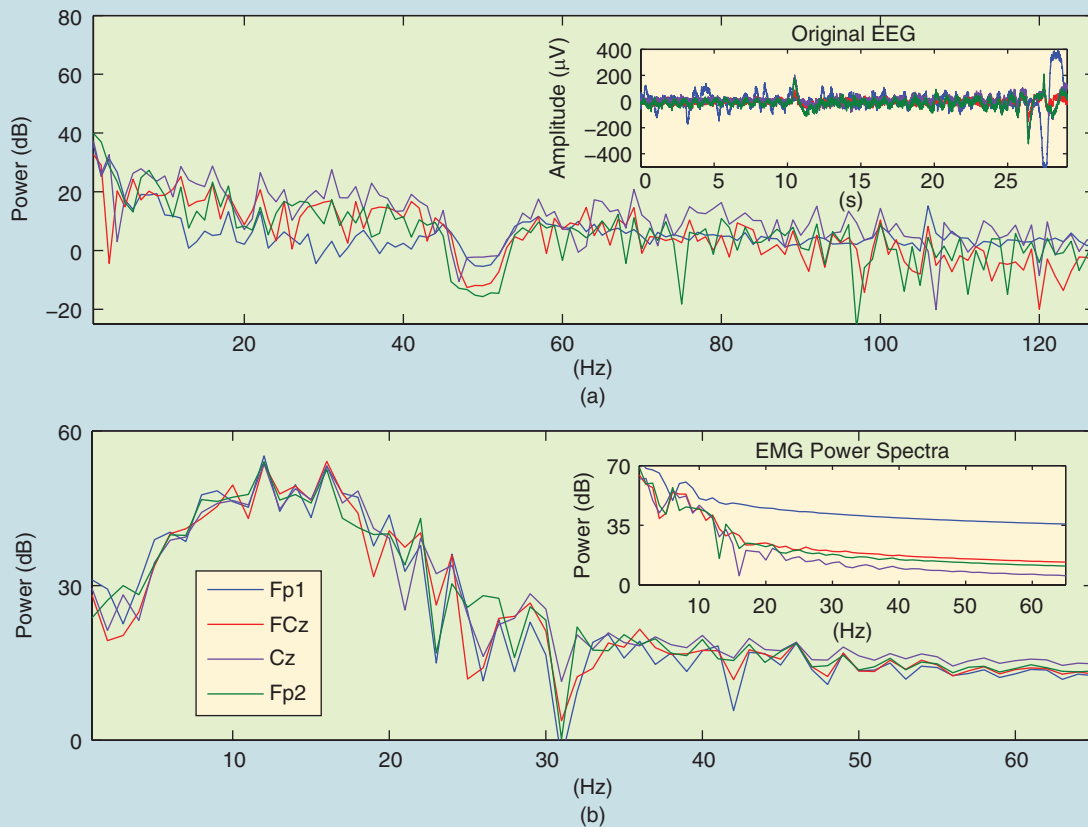
[FIG13] The MEMD versus ICA applied to four-channel EEG (Fp1, FCz, Fp2, Cz). (a) Power spectra of ICs IC1–IC4. (b) Power spectra of the IMFs containing the alpha EEG component. The ICs had no physical meaning, while both the EMG (≤ 2 Hz) and alpha (8–13 Hz) rhythm were localized meaningfully within the MEMD.

that the AM within IMFs is due to heterodyning. Another advantage is that EMD approaches are much less sensitive to data length (Figures 7 and 12), and do not require harmonics to model nonlinear signals as the AM/FM bases within EMD cater for intrawave modulations.

Our emphasis has been to illuminate the role of noise in EMD, its multidimensional and multivariate extensions, and several practical signal processing aspects in multivariate settings. The following are current and future directions in EMD research:

- EMD-inspired methods, including sparse monocomponent dictionaries, constrained optimization, and connections with compressed sensing [46], [5], [12]
- EMD as a tool for preprocessing (denoising, orthogonalization) and sparsification (T-F sparsification for tensors, ICA, machine learning)
- mathematical formalism for EMD establishing the extent to which postprocessing improves IMF conditioning, and the theory of EMD-enabled filterbanks
- completeness of bases for multivariate data-driven approaches and their mathematical foundation
- dealing with multivariate data channels with dynamical power imbalance, and further work on stoppage criteria, envelope interpolation, and HHS for multivariate data
- given an imminent release of EMD hardware, the end-effects and segment length issues also need revisiting

- scale-wise intrinsic measures for instantaneous synchrony, coherence, entropy, and causality.

The available software resources include MATLAB codebase for EMD and EEMD [49], [50], resources for MEMD [51], while some applications in brain science can be found in [48].

AUTHORS

Danilo P. Mandic (d.mandic@imperial.ac.uk) is a professor of signal processing at Imperial College London, United Kingdom. He has been working on multivariate and nonlinear signal processing, data-driven signal analysis, and adaptive multidimensional learning systems. He has authored two research monographs, been a guest professor at KU Leuven, Belgium, and a frontier researcher at RIKEN, Japan. He has also been a member of the IEEE Technical Committee on Signal Processing Theory and Methods and is an associate editor of *IEEE Signal Processing Magazine*, *IEEE Transactions on Signal Processing*,

and *IEEE Transactions on Neural Networks and Learning Systems*. He is a Fellow of the IEEE.

Naveed ur Rehman (nrehman.comsats@gmail.com) received the B.Eng. degree in electrical engineering from the National University of Sciences and Technology, Pakistan. He completed his Ph.D. degree in signal processing in 2011 from Imperial College, London, United Kingdom. He is currently working as an assistant professor in COMSATS Institute of Information Technology, Islamabad, Pakistan. His research interests include developing data adaptive multivariate T-F algorithms, nonlinear methods, and their applications in biomedical engineering, communications, remote sensing, data fusion, and renewable energy.

Zhaohua Wu (zwu@fsu.edu) received his B.S. degree from Nanjing University, China, in 1988 and his Ph.D. degree in atmospheric sciences from the University of Washington in 1998. He is an assistant professor of meteorology at Florida State University. His research interests are in atmospheric dynamics and climatic dynamics, as well as in the development of adaptive and local data analysis methods and applications of these methods to many fields. He received the 2007 Goddard Technology Award and the very first Hilbert–Huang Transform Award in 2011.

Norden E. Huang (norden@ncu.edu.tw) is the KT Lee Chair professor at the National Central University and the funding director of the Research Center for Adaptive Data Analysis. He is the inventor of the EMD method. For this invention, he received the 1998 NASA Special Space Act Award. He is a member of the U.S. National Academy of Engineering, an academician of Academia Sinica, and a foreign member of the Chinese Academy of Engineering.

REFERENCES

[1] D. Gabor, "Theory of communication," *J. IEE, Part III: Radio Commun. Eng.*, vol. 93, no. 26, pp. 429–441, 1946.

[2] E. Bedrosian, "A product theorem for Hilbert transforms," *Proc. IEEE*, vol. 51, no. 5, pp. 868–869, 1963.

[3] A. H. Nuttall and E. Bedrosian, "On the quadrature approximation to the Hilbert transform of modulated signals," *Proc. IEEE*, vol. 54, no. 10, pp. 1458–1459, 1966.

[4] S. Olhede and A. T. Walden, "The Hilbert spectrum via wavelet projections," *Proc. Roy. Soc. London A*, vol. 460, no. 2044, pp. 955–975, 2004.

[5] I. Daubechies, J. Lu, and H.-T. Wu, "Synchrosqueezing wavelet transforms: An empirical mode decomposition-like tool," *Appl. Comput. Harmon. Anal.*, vol. 30, no. 2, pp. 243–261, 2011.

[6] E. Sejdic, I. Djurovic, and L. Stankovic, "Quantitative performance analysis of scalogram as instantaneous frequency estimator," *IEEE Trans. Signal Processing*, vol. 56, no. 8, pp. 3837–3845, 2008.

[7] J. Tukey, *Exploratory Data Analysis*. Reading, MA: Addison-Wesley, 1977.

[8] B. Boashash, "Estimating and interpreting the instantaneous frequency of a signal," (Parts 1 and 2), *Proc. IEEE*, vol. 80, no. 4, pp. 520–568, 1992.

[9] X. Chen, Z. Wu, and N. E. Huang, "The time-dependent intrinsic correlation based on EMD," *Adv. Adapt. Data Anal.*, vol. 2. no. 2, pp. 233–266, 2010.

[10] N. E. Huang, Z. Shen, S. R. Long, M. C. Wu, H. H. Shih, Q. Zheng, N.-C. Yen, C. C. Tung, and H, H. Liu "The empirical mode decomposition and the Hilbert spectrum for nonlinear and non-stationary time series analysis," *Proc. Roy. Soc. London A*, vol. 454, no. 1971, pp. 903–995, 1998.

[11] G. Wang, X. Chen, F.-L. Qiao, Z. Wu, and N. E. Huang, "On intrinsic mode function," *Adv. Adapt. Data Anal.*, vol. 2, no. 3, pp. 277–293, 2010.

[12] T. Y. Hou and Z. Shi, "Adaptive data analysis via sparse time-frequency representation," *Adv. Adapt. Data Anal.*, vol. 3, no. 1, pp. 1–28, 2011.

[13] T. Y. Hou and Z. Shi, "Data driven time frequency analysis," *Appl. Comput. Harm. Anal.*, to be published.

[14] N. E. Huang, M.-L. C. Wu, S. R. Long, S. S. P Shen, W. Qu, P. Gloersen, and K. L. Fan "A confidence limit for the empirical mode decomposition and Hilbert spectral analysis," *Proc. Roy. Soc. London A*, vol. 459, no. 2037, pp. 2317–2345, 2003.

[15] P. Flandrin, G. Rilling, and P. Goncalves, "Empirical mode decomposition as a filter bank," *IEEE Signal Process. Lett.*, vol. 11, no. 2, pp. 112–114, 2004.

[16] R. N. Meeson, Jr., "HHT sifting and filtering," in *Hilbert-Huang Transform and Its Applications*, N. E. Huang and S. S. S. Shen, Eds. Singapore: World Scientific, 2005, pp. 75–105.

[17] Y. Kopsinis and S. McLauglin, "Improved EMD using doubly-iterative sifting and high order spline interpolation," *EURASIP J. Adv. Signal Process.*, vol. 2008, pp. 1–8, Mar. 2008.

[18] B. Huang and A. Kunoth, "An optimisation based EMD scheme," *J. Comput. Appl. Math.*, vol. 240, pp. 174–183, Mar. 2013.

[19] N. Huang, Z. Wu, S. Long, K. Arnold, X. Chen, and K. Blank, "On instantaneous frequency," *Adv. Adapt. Data Anal.*, vol. 1, no. 2, pp. 177–229, 2009.

[20] G. Rilling and P. Flandrin, "One or two frequencies? The EMD answers," *IEEE Trans. Signal Processing*, vol. 56, no. 1, pp. 85–95, 2008.

[21] H.-T. Wu, P. Flandrin, and I. Daubechies, "One or two frequencies? The synchrosqueezing answers," *Adv. Adapt. Data Anal.*, vol. 3, nos. 1 and 2, pp. 329–339, 2011.

[22] R. Deering and J. F. Kaiser, "The use of a masking signal to improve empirical mode decomposition," in *Proc. ICASSP*, 2005, pp. 485–488.

[23] Z. Wu and N. E. Huang, "Ensemble empirical mode decomposition: A noise-assisted data analysis method," *Adv. Adapt. Data Anal.*, vol. 1, no. 1, pp. 1–41, 2009.

[24] D. Looney and D. P. Mandic, "Multi-scale image fusion using complex EMD," *IEEE Tran. Signal Processing*, vol. 57, no. 4, pp. 1626–1630, 2009.

[25] T. Tanaka and D. P. Mandic, "Complex empirical mode decomposition," *IEEE Signal Process. Lett.*, vol. 14, no. 2, pp. 101–104, Feb. 2007.

[26] G. Rilling, P. Flandrin, P. Goncalves, and J. Lilly, "Bivariate empirical mode decomposition," *IEEE Signal Process. Lett.*, no. 12, vol. 14, pp. 936–939, 2007.

[27] M. Altaf and D. P. Mandic, "Rotation invariant empirical mode decomposition," in *Proc. ICASSP'07*, 2007, pp. 1009–1012.

[28] N. U. Rehman and D. P. Mandic, "Multivariate empirical mode decomposition," *Proc. Roy. Soc. London A*, vol. 466, no. 2117, pp. 1291–1302, 2010.

[29] N. U. Rehman and D. P. Mandic, "Empirical mode decomposition for trivariate signals," *IEEE Trans. Signal Processing*, vol. 59, no. 5, pp. 2421–2426, 2011.

[30] J. Cui and W. Freeden, "Equidistribution on the sphere," *SIAM J. Sci. Comput.*, vol. 18, no. 2, pp. 595–609, 1997.

[31] N. Rehman and D. P. Mandic, "Filterbank property of multivariate EMD," *IEEE Trans. Signal Processing*, vol. 59, no. 5, pp. 2421–2426, 2011.

[32] A. Linderhed, "Image EMD: A new tool for image processing," *Adv. Adapt. Data Anal.*, vol. 1, no. 2, pp. 265–294, 2009.

[33] J. Nunes, Y. Bouaoune, E. Delechelle, O. Niang, and Ph. Bunel, "Image analysis by bidimensional empirical mode decomposition," *Image Vis. Comput.*, vol. 21, no. 12, pp. 1019–1026, 2003.

[34] H. Wang, Z. Su, J. Cao, Y. Wang, and H. Zhang, "Empirical mode decomposition on surfaces," *Graph. Models*, vol. 74, no. 4, pp. 173–184, 2012.

[35] R. Pabel, R. Koch, G. Jager, and A. Kunoth, "Fast empirical mode decompositions of multivariate data based on adaptive spline-wavelets and a generalization of the Hilbert–Huang transformation (HHT) to arbitrary space dimensions," *Adv. Adapt. Data Anal.*, vol. 3, no. 2, pp. 337–358, 2010.

[36] C. Damerval, S. Meignen, and V. Perrier, "A new formulation for empirical mode decomposition based on constrained optimization," *IEEE Signal Process. Lett.*, vol. 14, no. 12, pp. 932–935, 2007.

[37] Y. Xu, B. Liu, J. Liu, and S. Riemenschneider, "Two-dimensional empirical mode decomposition by finite elements," *Proc. Roy. Soc. London A*, vol. 462, no. 2074, pp. 3081–3096, 2006.

[38] S. Meignen and V. Perrier, "A fast algorithm for bidimensional EMD," *IEEE Signal Process. Lett.*, vol. 12, no. 10, pp. 701–704, 2005.

[39] Z. Wu, N. Huang, and X. Chen, "The multidimensional ensemble empirical mode decomposition method," *Adv. Adapt. Data Anal.*, vol. 1, no. 3, pp. 339–372, 2009.

[40] A. Ahrabian, N. Rehman, and D. P. Mandic, "Bivariate EMD for unbalanced signals," *IEEE Signal Process. Lett.*, vol. 20, no. 3, pp. 245–248, 2013.

[41] D. Looney and D. P. Mandic, "A machine learning enhanced empirical mode decomposition," in *Proc. ICASSP*, 2008, pp. 1897–1900.

[42] D. P. Mandic and V. S. L. Goh, *Complex Valued Nonlinear Adaptive Filters: Noncircularity, Widely Linear and Neural Models*. Hoboken, NJ: Wiley, 2009.

[43] G. Rilling and P. Flandrin, "Sampling effects on the EMD," *Adv. Adapt. Data Anal.*, vol. 1, no. 1, pp. 43–59, 2009.

[44] P. J. Loughlin and B. Tacer, "Comments on the interpretation of instantaneous frequency," *IEEE Signal Process. Lett.*, vol. 4,, no. 5, pp. 123–125, 1997.

[45] D. Wei and A. Bovik, "On the instantaneous frequencies of multicomponent AM-FM signals," *IEEE Signal Process. Lett.*, vol. 5, no. 4, pp. 84–86, 1998.

[46] J. Smith, "The local mean decomposition and its application to EEG perception data," *J. Roy. Soc. Interface*, vol. 22, no. 5, pp. 443–454, 2005.

[47] T. M. Rutkowski, A. Cichocki, T. Tanaka, D. P. Mandic, J. Cao, and A. L. Ralescu, "Multichannel spectral pattern separation—An EEG processing application," in *Proc. ICASSP'09*, 2009, pp. 373–376.

[48] [Online]. Available: http://www.tara.tsukuba.ac.jp/~tomek/Welcome.html

[49] [Online]. Available: http://rcada.ncu.edu.tw/research1.htm

[50] [Online]. Available: http://perso.ens-lyon.fr/patrick.flandrin/software2.html

[51] [Online]. Available: http://www.commsp.ee.ic.ac.uk/~mandic/research/emd.htm

[SP]